

Spatial Discretizations-I : Local Methods

Ram D. Nair

Institute for Mathematics Applied to Geosciences (IMAGe)
Computational Information Systems Laboratory

National Center for Atmospheric Research, Boulder, CO 80305

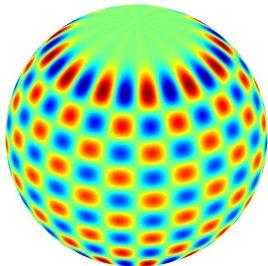
[Dynamical Core Model Intercomparison Project 2016 Workshop
June 6th – 17th, NCAR, Boulder, CO]



Global & Local Numerical Methods

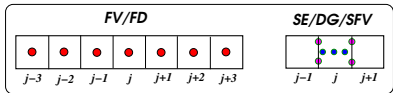
- **Global Methods:**

- Every point is “spectrally” connected to all other points in the domain
- Numerical method based on this idea is not suitable (efficient) for the current massively parallel architecture.
- E.g: global spectral methods (spherical harmonics) etc.



- **Local Methods:**

- Every point is “locally” connected to neighboring points in the domain
- The numerical methods based on local data access offer great parallel efficiency
- E.g: Compact FV/FD methods, element-based Galerkin methods.



Local Methods-I: Godunov-Type Finite-Volume Methods

- Godunov-type FV methods involve 3 major steps: Reconstruction, Evolution and Projection
- **Reconstruction step:** Piecewise polynomials are reconstructed over the grid cells spanning the domain from the known cell averages (piecewise constant data) at the previous time level (*van Leer 1974; Colella and Woodward 1984*).
- **Evolution step:** The piecewise polynomials are advanced in time, following the underlying conservation law.
- **Projection step:** New cell averages are computed on each cell by projecting the evolved polynomials onto cell averages.
- **Upwind FV**
 - Requires Riemann solvers, may need characteristic decomposition of the hyperbolic system
 - Accuracy and efficiency of the scheme is tied-up with the Riemann solvers
 - E.g.: Godunov (1st-O), MUSCL (2nd-O), PPM (3rd-O), ENO, ..
- **Central FV**
 - No Riemann solver or characteristic decomposition is required
 - Evolution at the cell edges, requires a staggered (dual) grid system
 - A system of PDEs can be solved component-wise, but more dissipative
 - E.g.: LxF (1st-O), Nessyahu-Tadmor (NT, 2nd-O), C-WENO
- **Our Interest:** Unstaggered upwind-based Godunov-type FV

Hyperbolic Conservation Laws

- Conservation laws are systems of nonlinear partial differential equations (PDEs) on **conservation (flux) form** and can be written:

$$\frac{\partial}{\partial t} U(\mathbf{x},t) + \sum_{j=1}^3 \frac{\partial}{\partial x_j} F_j(U, \mathbf{x}, t) = S(U),$$

where

- $U(\mathbf{x},t)$ is a vector function in 3D space coordinate \mathbf{x} and time $t > 0$.
- F_j are given flux vectors dependent on (U, \mathbf{x}, t) and include diffusive and convective effects
- $S(U)$ is the source term
- E.g: **Navier-Stokes equations** for compressible and incompressible flows can be written in this form with U representing mass, momentum and energy, $S(U)$ representing exterior forces.
- A large class of atmospheric equations of motion can be cast in this form.
- Scalar conservation law (e.g., mass continuity equation):

$$\frac{\partial \rho}{\partial t} + \nabla \cdot (\rho \mathbf{V}) = 0$$

Conservation Law: 1D Case

- 1D conservation law:

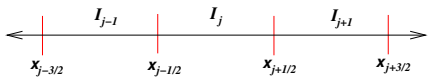
$$\begin{aligned}\frac{\partial U}{\partial t} + \frac{\partial F(U)}{\partial x} &= 0 \quad \text{in } D \times (0, T), \\ U_0(x) &= U(x, t = 0), \quad \forall x \in D\end{aligned}$$

- $F(U)$ is the flux (e.g: $F(U) = cU$ linear advection, $F(U) = U^2/2$, for Burgers' Equation)

Define the cell average on

$I_j, j = 1, \dots, N$:

$$\overline{U}_j(t) = \frac{1}{\Delta x_j} \int_{x_{j-1/2}}^{x_{j+1/2}} U(x, t) dx$$



$$\Delta x_j = x_{j+1/2} - x_{j-1/2}, \quad x_j = (x_{j+1/2} + x_{j-1/2})/2$$

- **Integral form:** Integrating over a cell I_j for a time interval $[t, t + \Delta t] \Rightarrow$

$$\overline{U}_j(t + \Delta t) = \overline{U}_j(t) - \frac{1}{\Delta x} \left[\int_{\tau=t}^{t+\Delta t} F(U(x_{j+1/2}, \tau)) d\tau - \int_{\tau=t}^{t+\Delta t} F(U(x_{j-1/2}, \tau)) d\tau \right]$$

- Semi-discrete form on a cell I_j :

$$\frac{d}{dt} \overline{U}_j(t) = - \frac{F_{j+1/2}(t) - F_{j-1/2}(t)}{\Delta x}, \quad \text{where } F_{j+1/2}(t) = \frac{1}{\Delta t} \int_t^{t+\Delta t} F(x_{j+1/2}, \tau) d\tau$$

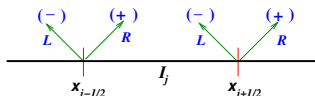
FV 1D Case: Reconstruction

- **Polynomial Reconstruction:** For a k^{th} order approximation, the solution $U(x)$ is approximated by a piecewise polynomial $P_j(x)$ of degree $k - 1$.

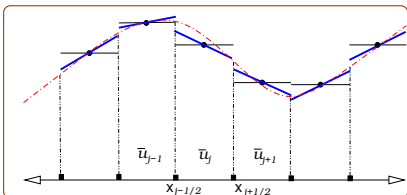
$$P_j(x) = U(x) + O(\Delta x^k), \text{ for } x \in I_j; \quad \frac{1}{\Delta x_j} \int_{x_{j-1/2}}^{x_{j+1/2}} P_j(\xi) d\xi = \bar{U}_j, \quad j = 1, 2, \dots, N.$$

$P_j(x)$ approximates $U(x)$ at the cell interfaces $x_{j \pm 1/2}$

$$U_{j+1/2}^- = P_j(x_{j+1/2}), \quad U_{j-1/2}^+ = P_j(x_{j-1/2})$$



- For Piecewise Linear Method (PLM) $P_j(\xi) = a_0 + a_1 \xi$
- For Piecewise Parabolic Method (PPM) $P_j(\xi) = a_0 + a_1 \xi + a_2 \xi^2$
- Coefficients a_i are derived using the conservation constraint $\int P_j(\xi) d\xi = \bar{U}_j \Delta x_j$



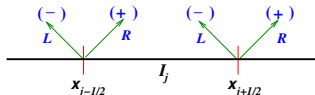
PLM reconstruction (van Leer, 1979)

Godunov-type FV Method: Numerical Flux

- For the Godunov-type FV Method, the approximate solution $P_j(x) \approx U(x)$ and the flux function $F(U)$ are not continuous at the cell interfaces.

At any interface $x_{j+1/2}$, $F(U)$ has “left” and “right” contributions:

$$F(U_{j+1/2}^-) \quad \text{and} \quad F(U_{j+1/2}^+)$$



- At the interface the physical flux $F(U)$ replaced with numerical flux $\hat{F}(U)$, by solving the Riemann problem:

$$\hat{F}_{j+1/2}(t) = \hat{F}(U_{j+1/2}^-(t), U_{j+1/2}^+(t))$$

- Choice for the numerical flux (Riemann solver):

- Several upwind-based numerical flux of varying complexity are available (e.g: Lax-Friedrichs (Rusanov), Roe, HLLC, AUSM_{up}⁺ etc.)
- For Advection:** Lax-Friedrichs flux is simple and efficient, but very diffusive for nonlinear problems.

$$\hat{F}_{j+1/2} = \frac{1}{2} \left[F(U_{j+1/2}^+) + F(U_{j+1/2}^-) - \alpha_{j+1/2} (U_{j+1/2}^+ - U_{j-1/2}^-) \right]$$

- For Euler system:** The AUSM_{up}⁺ flux by Liuo (2006) is suitable for atmospheric (low Mach number) modeling. (Ullrich et al. (2010), Chen et al. (2013))

Godunov-type FV Method: Time Integration

- Final form of the conservative Method:

$$\frac{\partial U}{\partial t} + \frac{\partial F(U)}{\partial x} = 0 \Rightarrow \frac{d}{dt} \bar{U}_j(t) = -\frac{\hat{F}_{j+1/2}(t) - \hat{F}_{j-1/2}(t)}{\Delta x}$$

- Solve the ODE

$$\frac{d}{dt} U = L(U) \quad \text{in } (0, T)$$

- A third-order strong stability preserving (SSP) Runge-Kutta scheme (*Gottlieb et al. 2001*)

$$\begin{aligned} U^{(1)} &= U^n + \Delta t L(U^n) \\ U^{(2)} &= \frac{3}{4}U^n + \frac{1}{4}U^{(1)} + \frac{1}{4}\Delta t L(U^{(1)}) \\ U^{n+1} &= \frac{1}{3}U^n + \frac{2}{3}U^{(2)} + \frac{2}{3}\Delta t L(U^{(2)}), \end{aligned}$$

- CFL stability (depends on the RK method)

$$\left| c \frac{\Delta t}{\Delta x} \right| \leq 1$$

FV: 2D Reconstruction

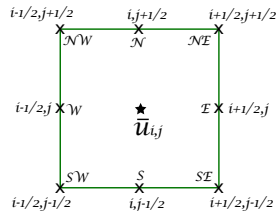
- Conservation Law 2D Case:

$$\frac{\partial U}{\partial t} + \frac{\partial F(U)}{\partial x} + \frac{\partial G(U)}{\partial y} = 0 \quad \text{OR} \quad \frac{\partial U}{\partial t} + \nabla \cdot \mathbf{F}(U) = 0, \text{ in } D \times (0, T], \forall x, y \in D$$

where the domain D is partitioned into non-overlapping cells C_{ij} ; $\mathbf{F} = (F, G)$

$$C_{ij} = [x_{i-1/2}, x_{i+1/2}] \otimes [y_{j-1/2}, y_{j+1/2}]$$

$$\Delta x_i = x_{i+1/2} - x_{i-1/2}, \quad \Delta y_j = y_{j+1/2} - y_{j-1/2}$$



- The 2D piecewise reconstruction polynomials $P(x, y)$ on each rectangular cell C_{ij} satisfies the conservation constraint,

$$\bar{U}_{ij}^n = \frac{1}{\Delta x_i \Delta y_j} \int_{y_{j-1/2}}^{y_{j+1/2}} \int_{x_{i-1/2}}^{x_{i+1/2}} P_{ij}(x, y) dx dy,$$

where \bar{U}_{ij}^n is the cell-average which evolves in time.

- Semi-discretized FV formulation can be obtained by the divergence theorem:

$$\frac{d\bar{U}_{ij}}{dt} = \frac{-1}{\Delta x_i \Delta y_j} \left[\sum_{k=1}^4 \int_{\Gamma_k} \hat{\mathbf{F}} \cdot \mathbf{n} \right],$$

where \mathbf{n} is the outward unit normal on cell boundary Γ_k .

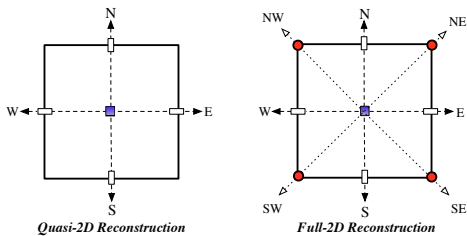
FV: 2D Reconstruction

- Accuracy of the multidimensional FV scheme is tied-up with the reconstruction polynomial and flux integrals

Flux integrals can be approximated with the Gauss quadrature of high-order accuracy,

$$\int_{\Gamma_k} \hat{\mathbf{F}} \cdot \mathbf{n} \approx |\Gamma_k| \sum_{l=1}^m \omega_l (\hat{\mathbf{F}} \cdot \mathbf{n})_l$$

ω_l is the quadrature weights.



- High-order FV scheme can be rigorously derived using high-order flux integrals and reconstruction functions, but at a higher computational cost
- E.g.: Fourth-order reconstruction polynomial (*Kruganov & Liu (2011), Katta et al., 2015*):

$$\begin{aligned} P(x,y) = & c_{0,0} + c_{1,0}x + c_{0,1}y + c_{2,0}x^2 + c_{0,2}y^2 + \\ & c_{1,1}xy + c_{2,1}x^2y + c_{1,2}xy^2 + c_{2,2}x^2y^2 + \\ & c_{3,0}x^3 + c_{0,3}y^3 + c_{4,0}x^4 + c_{0,4}y^4 \end{aligned}$$

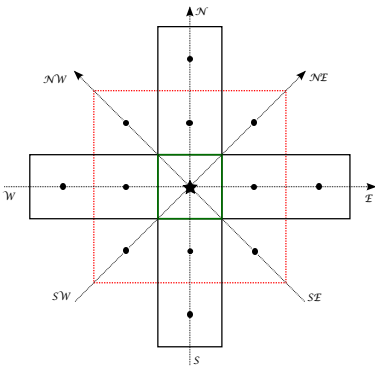
- E.g: Fully 2D fourth-order Shallow-water model by *Ullrich et al. (2010)*

FV 2D Reconstruction: 'Dimension-by-Dimension' Approach

- The idea is to combine two 1D reconstructions to form a 2D reconstruction on a cell C_{ij} .
- If $p(x,y)$ and $q(x,y)$ are two reconstruction functions on a cell C_{ij} , with cell average \bar{U}_{ij} :

$$R_{ij}(x,y) = \gamma p_{ij}(x,y) + (1 - \gamma)q_{ij}(x,y), \gamma \in [0, 1] \Rightarrow \frac{1}{\Delta x_i \Delta y_j} \int_{y_{j-1/2}}^{y_{j+1/2}} \int_{x_{i-1/2}}^{x_{i+1/2}} R_{ij}(x,y) dx dy = \bar{U}_{ij}$$

- For a cell C_{ij} : $\gamma_{i\pm 1/2, j\pm 1/2} = 0$, $\gamma_{i,j\pm 1/2} = \gamma_{i\pm 1/2, j} = 1$, i.e., $R(x,y) = \gamma p(x) + (1 - \gamma) q(y)$.



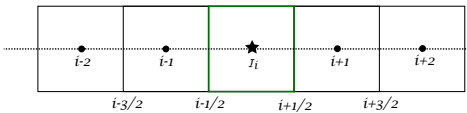
- Fully 2D 4th-order reconstruction requires two 5-cell wide halo with 13 cells, including corner cells. Multiple flux evaluation on each cell wall.
- Quasi-2D reconstruction requires two 5-cell wide halo with 9 cells,
- Advantage:** Computational economy (one flux evaluation per cell wall), easy to implement (e.g. Cubed-Sphere)
- Disadvantage:** Overall accuracy of the 'Quasi-2D' scheme may degrade to second-order accuracy

1D High-Order Reconstruction Schemes

- For 2D rectangular cells, the FV evolution equation simplifies to

$$\frac{d\bar{U}_{ij}}{dt} = \frac{-1}{\Delta x_i \Delta y_j} \left[\sum_{k=1}^4 \int_{\Gamma_k} \hat{\mathbf{F}} \cdot \mathbf{n} \right] \Rightarrow \frac{d}{dt} \bar{U}_{ij} = - \left[\frac{\hat{F}_{i+1/2,j} - \hat{F}_{i-1/2,j}}{\Delta x_i} + \frac{\hat{G}_{i,j+1/2} - \hat{G}_{i,j-1/2}}{\Delta y_j} \right]$$

- Fluxes $\hat{F}_{i\pm 1/2,j}$, $\hat{G}_{i,j\pm 1/2}$ are computed via high-order reconstruction
- We consider fifth-order accurate Weighted Essentially Non-Oscillatory (WENO5) 1D scheme [Shu (1997)]
- Piecewise Quartic Method or PQM (White & Adcroft, 2008) for reconstruction.



- For WENO5 required one 5-point stencil and $r = 3$ sub-stencils within
 - $S_0 = (i-2, i-1, i)$, $S_1 = (i-1, i, i+1)$
 - $S_2 = (i, i+1, i+2)$

- The WENO scheme uses a convex combination of nonlinear weights w_k from each stencil to produce non-oscillatory solution.
- WENO estimate at the interface $x_{i+1/2}$ for U is given by (Liu et al., 1994)

$$U_{i+1/2} = \sum_{k=0}^{r-1} w_k P_{i+1/2}^k \text{ where } P_{i+1/2}^k = \sum_{j=0}^{r-1} c_{kj} \bar{U}_{i-k+j}; \quad k = 0, \dots, r-1.$$

WENO5: Nonlinear Weights & Smoothness Indicator

- The nonlinear weights w_k depend on the “smoothness” indicator β_k :

$$w_k = \alpha_k / \sum_{s=0}^{r-1} \alpha_s, \quad \alpha_k = \frac{c_k}{(\varepsilon + \beta_k)^2}, \quad k = 0, \dots, r-1$$

where $c_0 = 3/10, c_1 = 3/5, c_2 = 1/10,$

- Smoothness indicator β_k (Shu, 1997). A smaller value of β_k indicates a smoother function

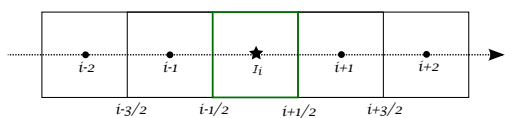
$$\begin{aligned}\beta_0 &= \frac{13}{12} (\bar{U}_i - 2\bar{U}_{i+1} + \bar{U}_{i+2})^2 + \frac{1}{4} (3\bar{U}_i - 4\bar{U}_{i+1} + \bar{U}_{i+2})^2, \\ \beta_1 &= \frac{13}{12} (\bar{U}_{i-1} - 2\bar{U}_i + \bar{U}_{i+1})^2 + \frac{1}{4} (\bar{U}_{i-1} - \bar{U}_{i+1})^2 \\ \beta_2 &= \frac{13}{12} (\bar{U}_{i-2} - 2\bar{U}_{i-1} + \bar{U}_i)^2 + \frac{1}{4} (\bar{U}_{i-2} - 4\bar{U}_{i-1} + 3\bar{U}_i)^2.\end{aligned}$$

- The values $U_{i+1/2}^\pm$ at the interfaces are evaluated from the reconstruction functions, followed by the numerical flux $\hat{F}_{i+1/2,j}, \hat{G}_{i,j+1/2}.$
- The final computation form of the conservation law is an ODE, can be solved R-K method.

$$\frac{d}{dt} \bar{U}_{ij} = - \left[\frac{\hat{F}_{i+1/2,j} - \hat{F}_{i-1/2,j}}{\Delta x_i} + \frac{\hat{G}_{i,j+1/2} - \hat{G}_{i,j-1/2}}{\Delta y_j} \right]$$

1D Piecewise Quartic Method (PQM): Reconstruction

- Natural extension of the Godunov method to high-order: $PCM < PLM < PPM < PQM$



- Employs 5-point compact stencil
- Potentially more efficient than WENO5
- Slope limiter can be used for monotonic option

- The Reconstruction polynomial for PQM (*White & Adcroft, 2008*)

$$P(x) = a_0 + a_1x + a_2x^2 + a_3x^4, \quad \int_{x_{i-1/2}}^{x_{i+1/2}} P(x) dx = \bar{U}_i$$

- Coefficients $a_k, k = 0, \dots, 3$ can be adjusted to make $P(x)$ monotonic (non-oscillatory)
- Fifth-order estimate for the edge values:

$$\begin{aligned} U_{i-1/2} &= \frac{1}{60}(-3\bar{U}_{i-2} + 27\bar{U}_{i-1} + 47\bar{U}_i - 13\bar{U}_{i+1} + 2\bar{U}_{i+2}) \\ U_{i+1/2} &= \frac{1}{60}(2\bar{U}_{i-2} - 13\bar{U}_{i-1} + 47\bar{U}_i + 27\bar{U}_{i+1} - 3\bar{U}_{i+2}) \end{aligned}$$

- The values $U_{i+1/2}^\pm$ at the interfaces are used for numerical flux $\hat{F}_{i+1/2,j}, \hat{G}_{i,j+1/2}$.

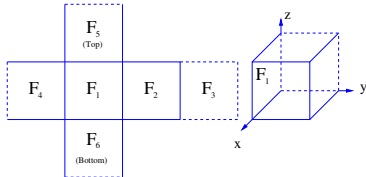
Extending CU-FV to the Cubed-Sphere Geometry

The Cubed-Sphere Topology [Sadourny (1972); Rancic et al. (1996)]

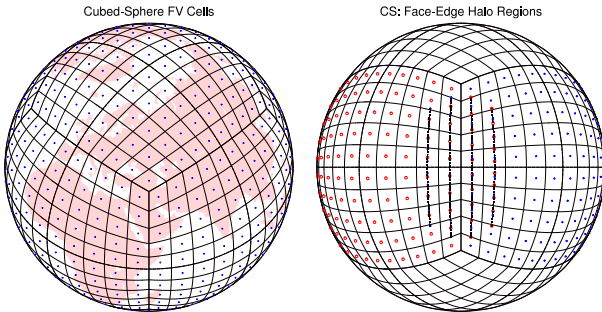
- Quasi-uniform rectangular mesh, logically square cells, well suited for cell-based FVM.
- Free of polar singularities. Non-orthogonal grid lines and discontinuous edges.
- Tensor form transport Eq. The metric term \sqrt{g} is known (analytic function).

$$\frac{\partial}{\partial t}(\sqrt{g}\phi) + \frac{\partial}{\partial x^1}(\sqrt{g}u^1\phi) + \frac{\partial}{\partial x^2}(\sqrt{g}u^2\phi) = 0; x^1, x^2 \in [-\pi/4, \pi/4] \Rightarrow$$

$$\frac{\partial \psi}{\partial t} + \frac{\partial F_1(\psi)}{\partial x^1} + \frac{\partial F_2(\psi)}{\partial x^2} = 0; (F_1, F_2) : \text{Contravariant Fluxes}, \psi = \sqrt{g}\phi.$$



Extending FV to Cubed-Sphere grid: Cubed-Sphere Edges



- Extend the gnomonic grid-lines x^1 or x^2 beyond the edges by two cells
- Cell-averages are interpolated (1D) onto the new halo cells along the x^2 or x^1 direction (*Katta & Nair, 2015*)
- The target halo cells are aligned along a great-circle arc, by the virtue of gnomonic projection
- “dimension-by-dimension” stencil avoids corner ghost cells, 1D 5-point stencil is used in both directions

FV: Bound-Preserving Filters for Transport

- Bound-preserving local filter (*Zhang & Shu, (2010), Zhang & Nair (2013)*)

$$\tilde{p}_{ij}(x,y) = \theta_{ij} p_{ij}(x,y) + (1 - \theta_{ij}) \bar{u}_{ij},$$

the limiter function $\theta_{ij} \in [0, 1]$, is defined as

$$\theta_{ij} = \min \left\{ \left| \frac{M - \bar{u}_{ij}}{M_{ij} - \bar{u}_{ij}} \right|, \left| \frac{m - \bar{u}_{ij}}{m_{ij} - \bar{u}_{ij}} \right|, 1 \right\},$$

where M and m are the global maximum and minimum values of the initial condition.

- The local extrema M_{ij} , m_{ij} are given by:

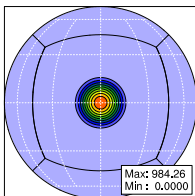
$$M_{ij} = \max_{(x,y) \in I_{ij}} \{p_{ij}(x,y)\}, \quad m_{ij} = \min_{(x,y) \in I_{ij}} \{p_{ij}(x,y)\}.$$

$\tilde{p}_{ij}(x,y)$ can be used for computing fluxes.

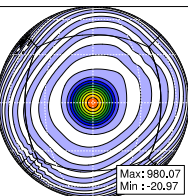
- For strict positivity (“zero” tolerance for negative values), Smolarkiewicz (1989) PP-filter is used at the final stage of FV discretization.

WENO5 scheme with Filter: [Cosine-bell Advection Test]

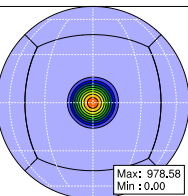
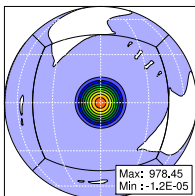
Demonstration of Filters: Cosine-Bell Advection Test
(a) Exact (Initial) Solution



(b) WENO-5

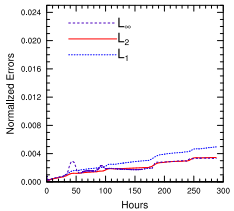


(c) WENO-5 wth BP

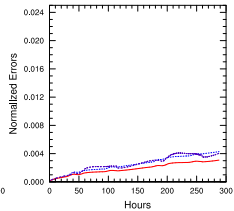


Normalized Errors: Cosine-Bell Advection Test

(a) WENO-5

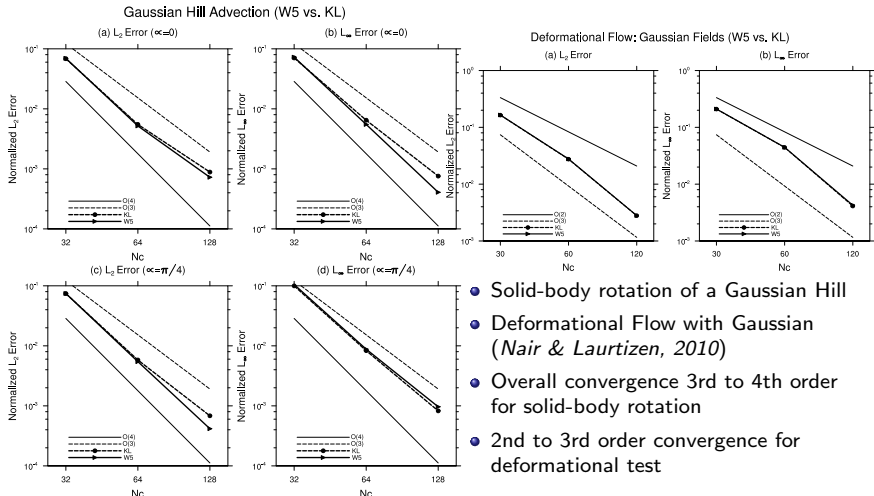


(b) KL



- Solid-body rotation of a cosine-bell (*Williamson et al. 1992*) with height $h \in [0, 1000]$.
- Flow (non-divergent) is along the NE direction ($\alpha = \pi/4$)
- After one revolution (12 days), $48 \times 48 \times 6$ cells & $CFL = 0.25$.
- Lax-Freiderichs numerical flux and RK3 time integration

WENO5, Convergence [Gaussian Hill Advection Test]



- Solid-body rotation of a Gaussian Hill
- Deformational Flow with Gaussian (*Nair & Lauritzen, 2010*)
- Overall convergence 3rd to 4th order for solid-body rotation
- 2nd to 3rd order convergence for deformational test

- Note: In terms of practical implementation (algorithmic simplicity), WENO5 is a clear winner because the underlying computational stencil is simple and does not require corner ghost cells.

Idealized Non-Hydrostatic Atmospheric Model: [2D Euler System]

- The 2D compressible Euler system in the x - z Cartesian geometry:

$$\frac{\partial}{\partial t} \mathbf{U} + \frac{\partial}{\partial x} \mathbf{F}(U) + \frac{\partial}{\partial z} \mathbf{G}(U) = \mathbf{S}(U)$$

where

$$\mathbf{U} = \begin{bmatrix} \rho \\ \rho u \\ \rho w \\ \rho \theta \end{bmatrix}, \mathbf{F} = \begin{bmatrix} \rho u \\ \rho u^2 + p \\ \rho uw \\ \rho u \theta \end{bmatrix}, \mathbf{G} = \begin{bmatrix} \rho w \\ \rho wu \\ \rho w^2 + p \\ \rho w \theta \end{bmatrix}, \mathbf{S} = \begin{bmatrix} 0 \\ 0 \\ -\rho g \\ 0 \end{bmatrix}.$$

- Based on conservation of momentum, mass and potential temperature, without Coriolis effect (rotation)
- Prognostic variables: ρ (density), (u, w) wind on (x, z) -plane, θ (potential temperature)
- $\theta = T(p_0/p)^{R_d/c_p}$, $p = C_0(\rho \theta)^\gamma$, where $C_0 = R_d^{1/\gamma} p_0^{-R_d/c_v}$; $\gamma = c_p/c_v$, $R_d = c_p - c_v = 287 \text{ J}/(\text{kg K})$, $g = 9.8 \text{ m}^2/\text{s}$, $p_0 = 10^5 \text{ Pa}$, $c_p = 1004 \text{ J kg}^{-1} \text{ K}^{-1}$, $c_v = 717 \text{ J kg}^{-1}$.

Idealized Non-Hydrostatic Atmospheric Model: [2D Euler System]

Ref: Giraldo & Restelli, JCP (2008); Norman et al., JCP (2010); Bao et al. MWR (2015)

- Decompose ρ , θ and p as the sum of a mean-state $(\bar{\cdot})$ and perturbation $(\cdot)'$: $\rho = \bar{\rho} + \rho'$, $\theta = \bar{\theta} + \theta'$ and $p = \bar{p} + p'$; such that $\frac{d\bar{p}}{dz} = -\bar{\rho}g$
- Hydrostatically balanced mean-state is ‘removed’ from the Euler system, resulting in:

$$\frac{\partial}{\partial t} \begin{bmatrix} \rho' \\ \rho u \\ \rho w \\ \rho \theta' \end{bmatrix} + \frac{\partial}{\partial x} \begin{bmatrix} \rho u \\ \rho u^2 + p' \\ \rho uw \\ \rho u\theta \end{bmatrix} + \frac{\partial}{\partial z} \begin{bmatrix} \rho w \\ \rho wu \\ \rho w^2 + p' \\ \rho w\theta \end{bmatrix} = \begin{bmatrix} 0 \\ 0 \\ -\rho'g \\ 0 \end{bmatrix}.$$

- The corresponding, CU-FV discretization for a control volume $C_{i,k}$:

$$\frac{d}{dt} \mathbf{U}_{i,k} = - \left[\frac{\mathbf{F}_{i+1/2,k} - \mathbf{F}_{i-1/2,k}}{\Delta x} + \frac{\mathbf{G}_{i,k+1/2} - \mathbf{G}_{i,k-1/2}}{\Delta z} + \mathbf{S}_{i,k} \right]$$

- Solve the above ODE with the third-order SSP-RK for $\mathbf{U} = [\rho', \rho u, \rho w, \rho \theta']^T$.

FV-NH: Numerical Fluxes for the Euler system

- Since the atmosphere flow is nearly incompressible, the corresponding Mach number is usually small (< 0.5). Classical Riemann solvers such as Lax-Friedrichs, HLLC etc., are very diffusive for low Mach flows
- Advection Upstream Splitting Method (AUSM⁺-up) by Liuo (2006) suitable for “all speeds” (Mach numbers). Recently used for atmospheric modeling (see, Ullrich (2010), Chen et al. (2013), Yang & Cai, 2014)
- AUSM⁺-up numerical flux: Split the numerical flux into a convective component and a pressure component

$$\hat{F}_{AUSM+up}(U^-, U^+) = F^{conv}(U^-, U^+) + F^{pres}(U^-, U^+)$$

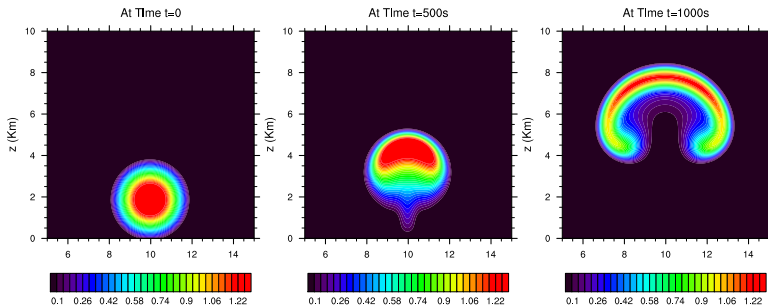
- For reference, we consider Lax-Friedrichs (Rusanov) flux:

$$\hat{F}_{LxF}(U^-, U^+) = \frac{1}{2}[(F(U^-) + F(U^+) - \alpha(U^+ - U^-)]$$

where α is the max value of the flux Jacobian, for NH system $\alpha = |u| + c$.

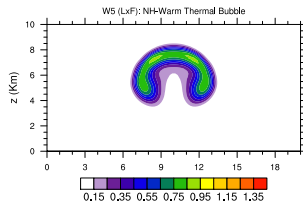
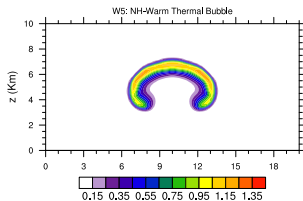
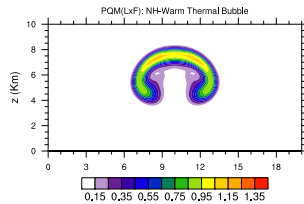
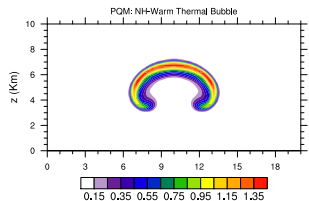
FV-NH: [2D NH Test Results]

Convective Thermal Bubble



- **Benchmark test:** A rising bubble (potential temperature perturbation θ') in a convectively neutral atmosphere (Wicker & Skamarock, 1998), simulated for 1000s.
- Initial potential temperature $\theta = \theta_0 + \Delta\theta \max(0, 1 - D/R)$; $\Delta\theta = 2\text{K}$, $\theta_0 = 300\text{K}$, $D = [(x - x_0)^2 + (y - y_0)^2]^{1/2}$, $R = 2\text{km}$, $x_0 = 10\text{km}$, $y_0 = 2\text{km}$, $u = w = 0$.
- The model domain is $[0, 20] \text{ km} \times [0, 10] \text{ km}$ and “no-flux” boundary conditions.

FV-NH, WENO5 and PQM: LxF vs AUSM Flux

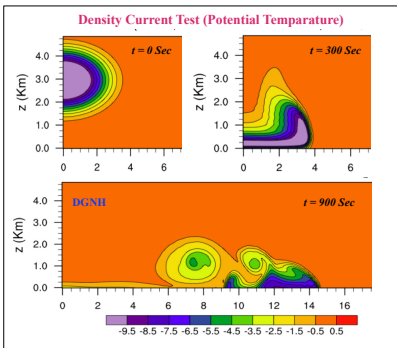


- The model domain is $[0,20]$ km $\times [0,10]$ km, and grid-spacing is uniformly set to $\Delta x = \Delta z = 200\text{m}$ such that $\text{CFL} \approx 0.7$, with "no-flux" boundary conditions.
- PQM is 1.5 times faster than WENO5 . LxF numerical flux is very diffusive not suitable for FV-NH modeling.

FV-NH: Straka Density Current

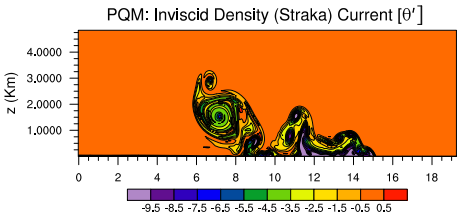
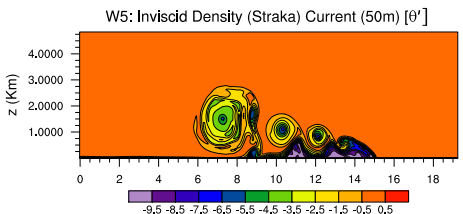
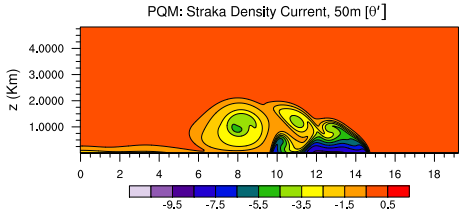
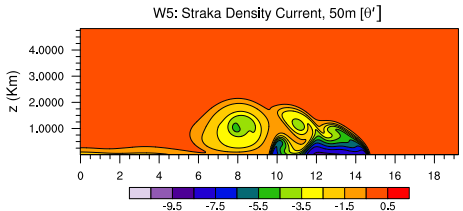
To validate Diffusion Process:

- Evolution of a cold bubble in a neutrally stratified atmosphere [Straka et al. (1993)].
- The cold bubble drops to the ground and forms 3 Kelvin-Helmholtz 'rotors' along the cold front at 900 sec.



- Domain $[-26.5, 26.5] \times [0, 6.4] \text{ km}^2$. $\theta = \bar{\theta} + \Delta\theta$;
- Initially, $\bar{\theta} = 300\text{K}$, $\Delta\theta = -15\text{K}$, $u = w = 0$.
- Simulated for 900 s, with diffusion ($v = 75.0 \text{ m}^2/\text{s.}$) added to the momentum and the potential temperature equations.
- No-flux boundary conditions ($\mathbf{u} \cdot \mathbf{n} = 0$) are used for all boundaries
- Note: Due to the symmetry, only half of the domain is shown

FV-NH Straka Density Current: with and without Explicit Diffusion



- Grid-converged solution at 50 m resolution with diffusion ($v = 75.0 \text{m}^2/\text{s.}$)
- Inviscid case: WENO5 is robust (expensive) even without explicit diffusive mechanism
- A combination of WENO5 and PQM would be a better option for practical application

Local Methods-II

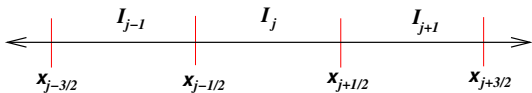
Element-Based Galerkin Methods

Discontinuous Galerkin Method (DGM) in 1D: Introduction

- 1D scalar conservation law:

$$\begin{aligned}\frac{\partial U}{\partial t} + \frac{\partial F(U)}{\partial x} &= 0 \quad \text{in } \Omega \times (0, T), \\ U_0(x) &= U(x, t = 0), \quad \forall x \in \Omega\end{aligned}$$

- E.g., $F(U) = cU$ (Linear advection), $F(U) = U^2/2$ (Burgers' Equation)
- The domain Ω (periodic) is partitioned into N_x non-overlapping elements (intervals) $I_j = [x_{j-1/2}, x_{j+1/2}]$, $j = 1, \dots, N_x$, and $\Delta x_j = (x_{j+1/2} - x_{j-1/2})$



DGM-1D: Weak Formulation

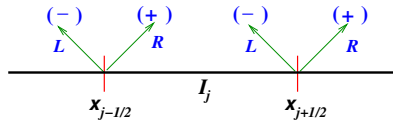
A **weak formulation** of the problem for the approximate solution U_h is obtained by multiplying the PDE by a *test function* $\varphi_h(x)$ and integrating over an element I_j :

$$\int_{I_j} \left[\frac{\partial U_h}{\partial t} + \frac{\partial F(U_h)}{\partial x} \right] \varphi_h(x) dx = 0, \quad U_h, \varphi_h \in \mathcal{V}_h$$

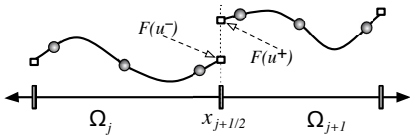
Integrating the second term by parts \implies

$$\begin{aligned} & \int_{I_j} \frac{\partial U_h(x,t)}{\partial t} \varphi_h(x) dx - \int_{I_j} F(U_h(x,t)) \frac{\partial \varphi_h}{\partial x} dx + \\ & F(U_h(x_{j+1/2},t)) \varphi_h(x_{j+1/2}^-) - F(U_h(x_{j-1/2},t)) \varphi_h(x_{j-1/2}^+) = 0, \end{aligned}$$

where $\varphi(x^-)$ and $\varphi(x^+)$ denote "left" and "right" limits.



DGM-1D: Flux term (“Gluing” the discontinuous element edges)



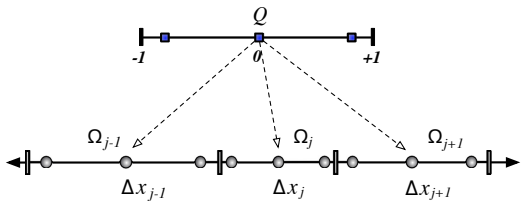
- Flux function $F(U_h)$ is **discontinuous** at the interfaces $x_{j\pm 1/2}$
- $F(U_h)$ is replaced by a **numerical flux** function $\hat{F}(U_h)$, dependent on the left and right limits of the discontinuous function U . At the interface $x_{j+1/2}$,

$$\hat{F}(U_h)_{j+1/2}(t) = \hat{F}(U_h(x_{j+1/2}^-, t), U_h(x_{j+1/2}^+, t))$$

- Typical flux formulae (**Approx. Riemann Solvers**): Gudunov, Lax-Friedrichs, Roe, HLLC, etc.
- Lax-Friedrichs numerical flux formula:-

$$\hat{F}(U_h) = \frac{1}{2} [(F(U_h^-) + F(U_h^+)) - \alpha(U_h^+ - U_h^-)].$$

DGM-1D: Space Discretization (Evaluation of the Integrals)



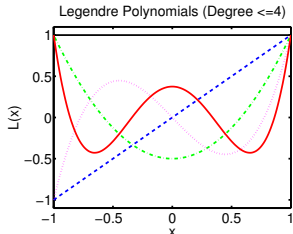
- Map every element Ω_j onto the reference element $[-1, +1]$ by introducing a local coordinate $\xi \in [-1, +1]$ s.t.,

$$\xi = \frac{2(x - x_j)}{\Delta x_j}, x_j = (x_{j-1/2} + x_{j+1/2})/2 \Rightarrow \frac{\partial}{\partial x} = \frac{2}{\Delta x_j} \frac{\partial}{\partial \xi}.$$

- Use a high-order Gaussian quadrature such as the Gauss-Legendre (GL) or Gauss-Lobatto-Legendre (GLL) quadrature rule. The GLL quadrature is 'exact' for polynomials of degree up to $2N - 1$.

$$\int_{-1}^1 f(\xi) d\xi \approx \sum_{n=0}^N w_n f(\xi_n); \quad \text{for GLL, } \xi_n \Leftarrow (1 - \xi^2) P'_\ell(\xi) = 0$$

DGM-1D: Representation of Test function & Approximate Solution



- The model basis set for the \mathcal{P}^k DG method consists of Legendre polynomials, $\mathcal{B} = \{P_\ell(\xi), \ell = 0, 1, \dots, k\}$.
- Test function $\varphi_h(x)$ and approximate solution $U_h(x)$ belong to \mathcal{B}

$$U_h(\xi, t) = \sum_{\ell=0}^k U_h^\ell(t) P_\ell(\xi) \quad \text{for } -1 \leq \xi \leq 1, \quad \text{where}$$

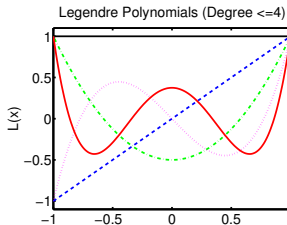
$$U_h^\ell(t) = \frac{2\ell+1}{2} \int_{-1}^1 U_h(\xi, t) P_\ell(\xi) d\xi \quad \ell = 0, 1, \dots, k.$$

$$\int_{-1}^1 P_m(x) P_n(x) dx = \frac{2}{2m+1} \delta_{m,n} \Leftarrow \text{Orthogonality}$$

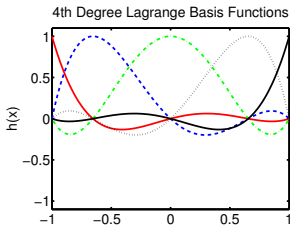
- $U_h^\ell(t)$ is the degrees of freedom (dof) evolves w.r.t time.

DGM-1D: Orthogonal Basis Set (Modal Vs Nodal)

Modal basis functions



Nodal basis functions



- The **nodal** basis set \mathcal{B} is constructed using Lagrange-Legendre polynomials $h_i(\xi)$ with roots at Gauss-Lobatto quadrature points (**physical space**).

$$U_j(\xi) = \sum_{j=0}^k U_j h_j(\xi) \quad \text{for } -1 \leq \xi \leq 1,$$

$$h_j(\xi) = \frac{(\xi^2 - 1)P'_k(\xi)}{k(k+1)P_k(\xi_j)(\xi - \xi_j)}, \quad \int_{-1}^1 h_i(\xi)h_j(\xi) = w_i \delta_{ij}.$$

- Nodal version was shown to be more computationally efficient than the Modal version (see, Levy, Nair & Tufo, Comput. & Geos. 2007)
- Modal version is more “friendly” with monotonic limiting

Time Integration

- Finally, the **weak formulation** leads the PDE to the time dependent ODE

$$\int_{I_j} \left[\frac{\partial U_h}{\partial t} + \frac{\partial F(U_h)}{\partial x} \right] \varphi_h(x) dx = 0 \quad \Rightarrow \quad \frac{d}{dt} U_h^\ell(t) = \mathcal{L}(U_h) \quad \text{in } (0, T) \times \Omega$$

For Nodal case:

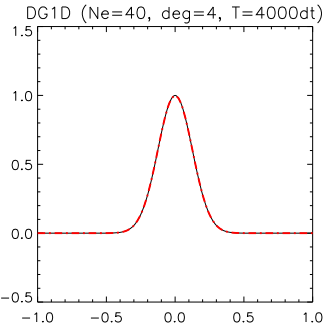
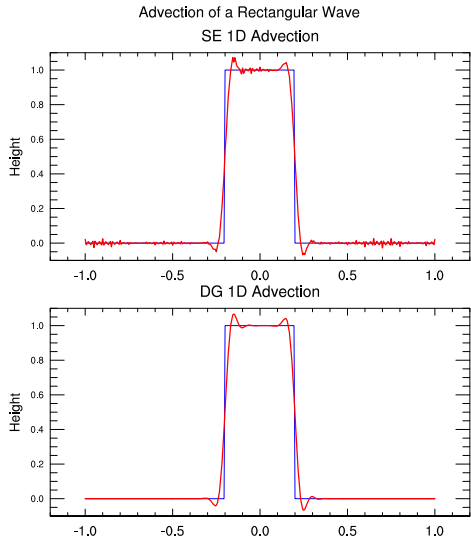
$$\frac{d}{dt} U_h(t) = \mathcal{L}(U_h) \quad \text{in } (0, T) \times \Omega$$

- Strong Stability Preserving third-order Runge-Kutta (SSP-RK) scheme (*Gottlieb et al., SIAM Review, 2001*)

$$\begin{aligned} U^{(1)} &= U^n + \Delta t \mathcal{L}(U^n) \\ U^{(2)} &= \frac{3}{4} U^n + \frac{1}{4} U^{(1)} + \frac{1}{4} \Delta t \mathcal{L}(U^{(1)}) \\ U^{n+1} &= \frac{1}{3} U^n + \frac{2}{3} U^{(2)} + \frac{2}{3} \Delta t \mathcal{L}(U^{(2)}). \end{aligned}$$

- CFL for the DG scheme is **estimated** to be $1/(2k+1)$, where k is the degree of the polynomial (*Cockburn and Shu, 1989*).
- Remedy: Use low-order polynomials ($k \leq 3$) or efficient semi-implicit / implicit time integrators or high-order multi-stage R-K method.

DGM-1D: Results (Simple Linear Advection Test)



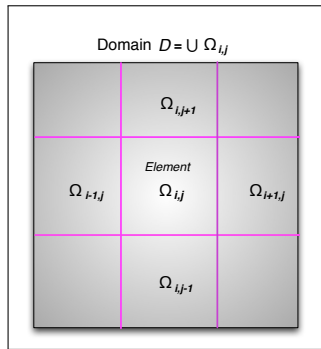
- DG Advantage: Smooth evolution of solution. DG has about 20% smaller time-step restriction compared to SE with explicit methods.
- SE and nodal form of DG use identical GLL grid system. Same MPI communication can be used.

DG Methods in 2D Cartesian Geometry

2D Scalar conservation law:

$$\frac{\partial U}{\partial t} + \nabla \cdot \mathbf{F}(U) = S(U), \quad \text{in } (0, T) \times \mathcal{D}; \quad \forall (x^1, x^2) \in \mathcal{D},$$

where $U = U(x^1, x^2, t)$, $\nabla \equiv (\partial/\partial x^1, \partial/\partial x^2)$, $\mathbf{F} = (F, G)$ is the flux function, and S is the source term.



- The domain \mathcal{D} is partitioned into non-overlapping elements $\Omega_{i,j}$
- Element edges are discontinuous
- Problem is locally solved on each element $\Omega_{i,j}$

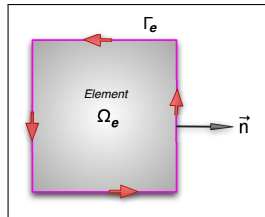
DG-2D Spatial Discretization for an Element Ω_e in \mathcal{D}

- Approximate solution U_h belongs to a vector space \mathcal{V}_h of polynomials $\mathcal{P}_N(\Omega_e)$.
- The **Galerkin formulation**: Multiplication of the basic equation by a *test function* $\varphi_h \in \mathcal{V}_h$ and integration over an element Ω_e with boundary Γ_e ,

$$\int_{\Omega_e} \left[\frac{\partial U_h}{\partial t} + \nabla \cdot \mathbf{F}(U_h) - S(U_h) \right] \varphi_h d\Omega$$

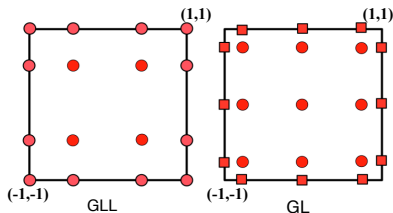
- **Weak Galerkin formulation** : Integration by parts (Green's theorem) yields:

$$\frac{\partial}{\partial t} \int_{\Omega_e} U_h \varphi_h d\Omega - \int_{\Omega_e} \mathbf{F}(U_h) \cdot \nabla \varphi_h d\Omega + \int_{\Gamma_e} \mathbf{F}(U_h) \cdot \vec{n} \varphi_h d\Gamma = \int_{\Omega_e} S(U_h) \varphi_h d\Omega$$



- The analytic flux $\mathbf{F}(U_h) \cdot \vec{n}$ must be replaced by a numerical flux such as the **local Lax-Friedrichs (Rusanov) Flux**:
- $$\mathbf{F}(U_h) \cdot \vec{n} = \frac{1}{2} [(\mathbf{F}(U_h^-) + \mathbf{F}(U_h^+)) \cdot \vec{n} - \alpha(U_h^+ - U_h^-)].$$
- α is the upper bound on the absolute value of eigenvalues of the **flux Jacobian** $\mathbf{F}'(U)$; usually α is the local max speed of the system.

DG Method: Nodal Spatial Discretization



- GLL and GL type 2D quadrature grid.
- Every element Ω_e is mapped onto a unique reference element $[-1, 1]^2$, with local coordinates $(\xi, \eta) \in [-1, 1]$.

- The nodal basis set $\{h_i(\xi) * h_j(\eta)\}$ contains tensor-product of Lagrange polynomials $h_i(\xi)$,

$$h_i(\xi)|_{\text{GLL}} = \frac{(\xi^2 - 1)P'_N(\xi)}{N(N+1)P_N(\xi_i)(\xi - \xi_i)} \quad \text{OR} \quad h_i(\xi)|_{\text{GL}} = \frac{P_{N+1}(\xi)}{P'_{N+1}(\xi_i)(\xi - \xi_i)},$$

where $P_N(\xi)$ is the N^{th} degree Legendre polynomial.

- The approximate solution and test functions are expressed in terms of basis function:

$$U_h(\xi, \eta) = \sum_{i=0}^N \sum_{j=0}^N U_{ij} h_i(\xi) h_j(\eta) \quad \text{for } -1 \leq \xi, \eta \leq 1$$

- Final form for the discretization leads to ODEs:

$$\frac{\partial U}{\partial t} + \nabla \cdot \mathbf{F}(U) = S(U) \quad \Rightarrow \quad \frac{d}{dt} U_h(t) = \mathcal{L}(U_h)$$

DG-2D, Diffusion Process: Advection-Diffusion Problem

Local Discontinuous Galerkin (LDG) method

- Diffusion: Extremely important for practical atmospheric models
 - Bassi and Rebay (JCP, 1997) introduced a scheme for treating diffusion (viscous flux) terms in DG discretization of the compressible Navier-Stokes equations.
 - Cockburn & Shu (1998) generalized this approach known as the LDG method.
-
- For the advection-diffusion equation on an element Ω , with known (constant) diffusion coefficient v .

$$\frac{\partial U}{\partial t} + \nabla \cdot \mathbf{F}(U) = v \nabla^2 U$$

- The key idea of LDG approach is the introduction of a local auxiliary variable $\mathbf{q} = v \nabla U$, and rewrite the above problem as a first-order system:

$$\begin{aligned}\mathbf{q} - v \nabla U &= 0 \\ \frac{\partial U}{\partial t} + \nabla \cdot \mathbf{F}(U) - \nabla \cdot \mathbf{q} &= 0\end{aligned}$$

- Discretize the above system employing the weak formulation (Green's method)

The Diffusion Process: LDG method

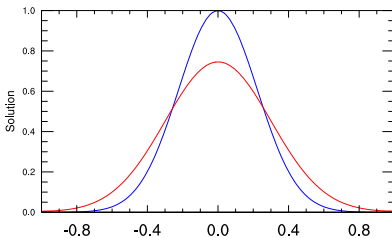
- Multiplying by a vector test function $\Phi \in \mathcal{V}^d(\Omega)$, and integrating by parts

$$\int_{\Omega} \mathbf{q} \cdot \Phi d\Omega = v \left[\int_{\partial\Omega} \mathbf{U}^* \Phi \cdot \vec{n} d\sigma - \int_{\Omega} U \nabla \cdot \Phi d\Omega \right]$$

- The weak formulation of advection-diffusion equation obtained using the test function ($\varphi \in \mathcal{V}(\Omega)$) and the Lax-Friedrichs flux $\hat{\mathbf{F}}$:

$$\begin{aligned} \frac{\partial}{\partial t} \int_{\Omega} U \varphi d\Omega & - \int_{\Omega} \mathbf{F}(U) \cdot \nabla \varphi d\Omega + \int_{\partial\Omega} \hat{\mathbf{F}}(U) \cdot \vec{n} \varphi d\sigma \\ & + \int_{\Omega} \mathbf{q} \cdot \nabla \varphi d\Omega - \int_{\partial\Omega} \mathbf{q}^* \cdot \vec{n} \varphi d\sigma = 0, \end{aligned}$$

DG 1D Advection-Diffusion



For the LDG method, numerical fluxes U^* , \mathbf{q}^* are defined in terms of jump $[\cdot]$ and central $\{\cdot\}$ fluxes:

$$\mathbf{U}^* = \{U\} + \beta \cdot [U], \quad \mathbf{q}^* = \{\mathbf{q}\} - \beta [\mathbf{q}] - \eta_k [U]$$

$$\{U\} = (U^+ + U^-)/2, [U] = (U^- - U^+)/\vec{n}$$

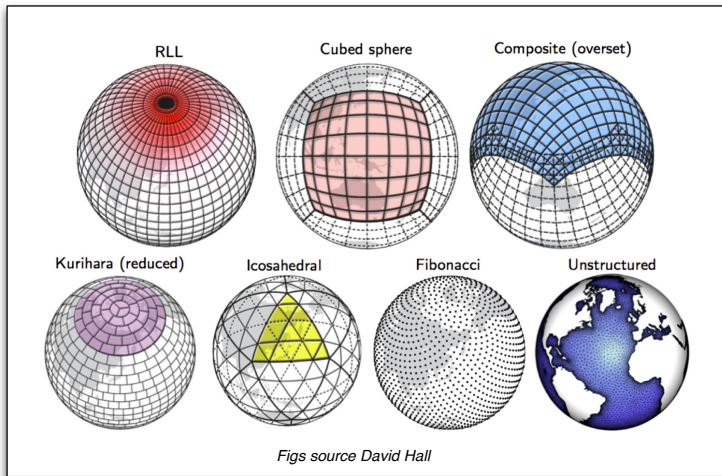
$$\{\mathbf{q}\} = (\mathbf{q}^+ + \mathbf{q}^-)/2, [\mathbf{q}] = (\mathbf{q}^- - \mathbf{q}^+) \cdot \vec{n}$$

Cockburn & Shu (1998)

Extending DG Methods to Spherical Geometry

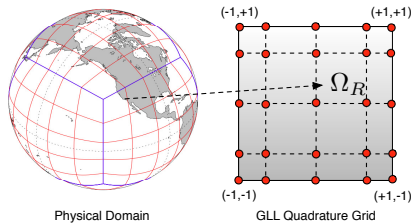
Various Spherical Grid Systems

- DG method can be potentially used on various spherical mesh with triangular or quadrilateral (or both) elements



HOMME Grid System: Local Mapping

Cubed-Sphere ($N_e = 5$) with 5×5 GLL points



- Each face of the cubed-sphere is partitioned into $N_e \times N_e$ rectangular non-overlapping elements.
- Total $6 \times N_e^2$ span the entire sphere.
- Each element is mapped onto the [Gauss-Lobatto-Legendre \(GLL\) reference element](#) defined by $-1 \leq \xi, \eta \leq 1$

- Flux is the only “communicator” at the element edges. Nearest neighbor communication is ideal for parallel implementation.

Shallow Water Equations (SWE): General Form

Spherical SWE are used as a test-bed for various numerical formulations of the horizontal aspects of 3D dynamics.

- Flux-Form SWE (Mass and Momentum conservative)

$$\begin{aligned}\frac{\partial h\mathbf{v}}{\partial t} + \nabla \cdot (\mathbf{v}h\mathbf{v} + \frac{1}{2}gh^2\mathbf{I}) &= -f\hat{\mathbf{k}} \times h\mathbf{v} - gh\nabla h_s, \\ \frac{\partial h}{\partial t} + \nabla \cdot (h\mathbf{v}) &= 0\end{aligned}$$

- Vector-Invariant (VI) form of SWE (Mass conservative)

$$\begin{aligned}\frac{\partial \mathbf{v}}{\partial t} + \nabla \left(\frac{\mathbf{v} \cdot \mathbf{v}}{2} \right) &= -(\zeta + f)\hat{\mathbf{k}} \cdot \mathbf{v} - \nabla \Phi \\ \frac{\partial h}{\partial t} + \nabla \cdot (h\mathbf{v}) &= 0\end{aligned}$$

- h depth of the fluid, \mathbf{v} is the velocity vector
- HOMME/DG has both implementations

SWE on the Cubed-Sphere: Vector-Invariant Form

On the cubed-sphere, SWE are written in following tensor form:

[Nair et al., (2005)]

$$\frac{\partial}{\partial t} \begin{bmatrix} \sqrt{G}h \\ u_1 \\ u_2 \end{bmatrix} + \frac{\partial}{\partial x^1} \begin{bmatrix} \sqrt{G}hu^1 \\ E \\ 0 \end{bmatrix} + \frac{\partial}{\partial x^2} \begin{bmatrix} \sqrt{G}hu^2 \\ 0 \\ E \end{bmatrix} = \begin{bmatrix} 0 \\ \sqrt{G}u^2(f + \zeta) \\ -\sqrt{G}u^1(f + \zeta) \end{bmatrix},$$

h is the height, f Coriolis term and Φ is the geopotential height. Energy term and vorticity are defined as

$$E = \Phi + \frac{1}{2}(u_1 u^1 + u_2 u^2), \quad \zeta = \frac{1}{\sqrt{G}} \left[\frac{\partial u_2}{\partial x^1} - \frac{\partial u_1}{\partial x^2} \right].$$

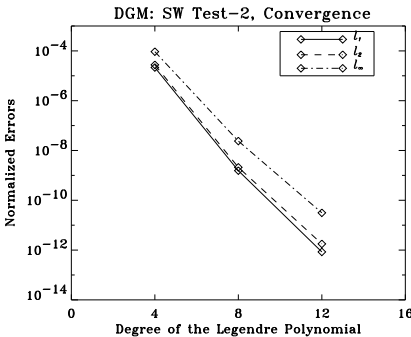
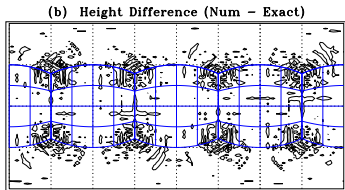
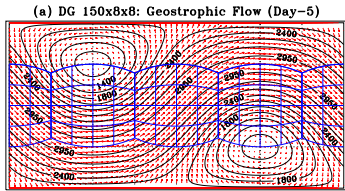
Metric tensor in terms of longitude-latitude (λ, θ) :

$$G_{ij} = A^T A; \quad A = \begin{bmatrix} R \cos \theta \partial \lambda / \partial x^1 & R \cos \theta \partial \lambda / \partial x^2 \\ R \partial \theta / \partial x^1 & R \partial \theta / \partial x^2 \end{bmatrix} \quad \begin{bmatrix} u \\ v \end{bmatrix} = A \begin{bmatrix} u^1 \\ u^2 \end{bmatrix};$$

The matrix A is used for transforming spherical (**physical**) velocity (u, v) to the **covariant** (u_1, u_2) and **contravariant** (u^1, u^2) velocity. $u_i = G_{ij} u^j$, $u^i = G^{ij} u_j$, and $G^{ij} = (G_{ij})^{-1}$, $G = |G_{ij}|$

SW Test-2: Geostrophic Flow (steady state)

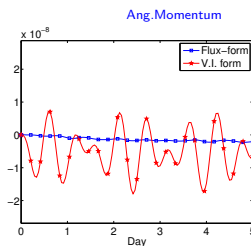
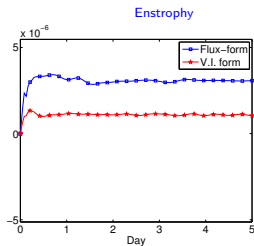
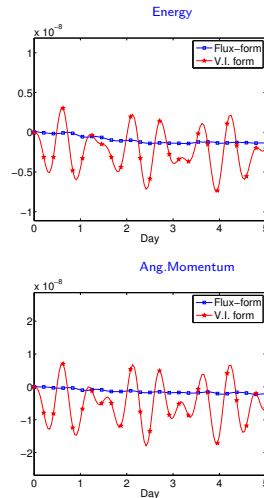
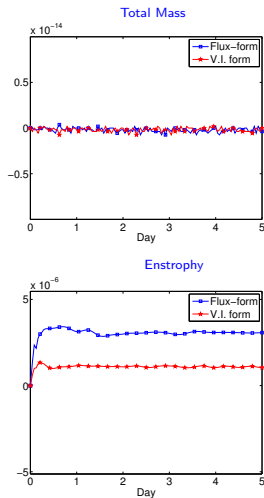
- High-order accuracy and spectral convergence



Steady state geostrophic flow ($\alpha = \pi/4$). Max height error is $\mathcal{O}(10^{-6})$ m.

(Nair et al., MWR 2005)

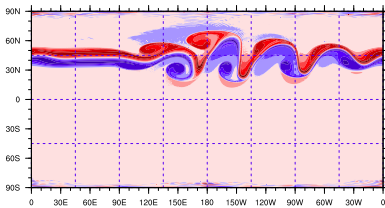
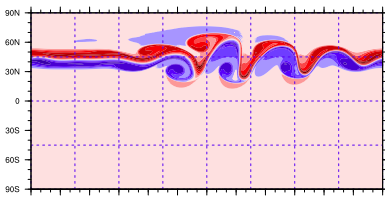
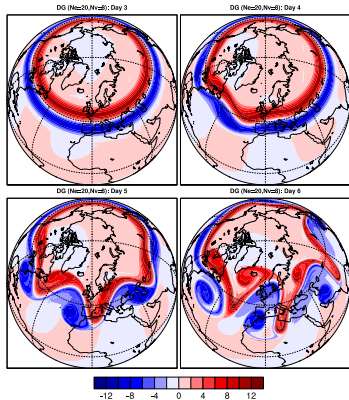
SWE, V-I vs Flux-Form: Conservation of Integral Invariants



- For the conservation of global invariants, the flux-form SW model shows better conservation of total energy and angular momentum [Bao, Nair & Tufo (JCP, 2013)]
- As far as the computational complexity is concerned, the vector-invariant form is simpler and more efficient.

SWE Flux-Form: Barotropic Instability Test [Galewsky et al. 2004]

- Effect of LDG Diffusion (second-order Laplacian)
- Relative vorticity field (ζ) for the barotropic instability test at day 6, with a resolution $\approx 0.43^\circ$ at the equator ($N_e = 30, N = 7$), with explicit time step $\Delta t = 5$ s.

LDG Diffusion, $\nu = 0$ LDG Diffusion, $\nu = 10^4 \text{ m}^2/\text{s}$ Barotropic Instability Test: Relative Vorticity Fields (10^{-5} s^{-1}), 0.6 deg

Vertical Aspects of Non-Hydrostatic Dynamics

Idealized Non-Hydrostatic Atmospheric Model: [2D Euler System]

- Based on conservation of momentum, mass and potential temperature (without Coriolis effect) the classical compressible 2D Euler system can be written in vector form:

$$\begin{aligned}\frac{\partial \rho}{\partial t} + \nabla \cdot (\rho \mathbf{u}) &= 0 \\ \frac{\partial \rho \mathbf{u}}{\partial t} + \nabla \cdot (\rho \mathbf{u} \otimes \mathbf{u} + p \mathbf{I}) &= -\rho g \mathbf{k} \\ \frac{\partial \rho \theta}{\partial t} + \nabla \cdot (\rho \theta \mathbf{u}) &= 0\end{aligned}$$

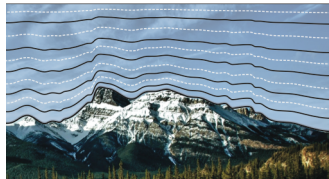
where ρ is the density, $\mathbf{u} = (u, w)$ the velocity vector such that $w = \mathbf{u} \cdot \mathbf{k}$, and θ the potential temperature. The pressure p and θ are related through the equation of state:

$$p = p_0 \left(\frac{\rho \theta R_d}{p_0} \right)^{c_p/c_v}; \quad p_0 = 10^5 \text{ Pa}, \quad R_d = 287 \text{ J/(kg K)}, \quad c_p/c_v = 1.4$$

- The 2D Euler system in the x - z Cartesian geometry can be written in flux-form:

$$\frac{\partial}{\partial t} \begin{bmatrix} \rho \\ \rho u \\ \rho w \\ \rho \theta \end{bmatrix} + \frac{\partial}{\partial x} \begin{bmatrix} \rho u \\ \rho u^2 + p \\ \rho uw \\ \rho u \theta \end{bmatrix} + \frac{\partial}{\partial z} \begin{bmatrix} \rho w \\ \rho wu \\ \rho w^2 + p \\ \rho w \theta \end{bmatrix} = \begin{bmatrix} 0 \\ 0 \\ -\rho g \\ 0 \end{bmatrix}.$$

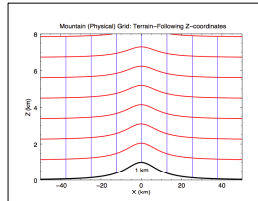
Terrain-Following z -Coordinates: $[(x, z) \rightarrow (x, \zeta)]$



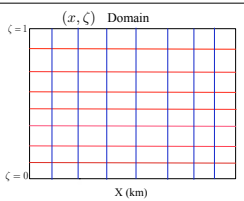
- Introduced by Gal-Chen & Somerville, JCP (1975).
- If $h = h(x)$ is the prescribed mountain profile and z_T is the top of the model domain,
- The (x, z) height coordinates can be transformed to (x, ζ) coordinates using the following relation, where ζ is monotonic.

$$\zeta = z_T \frac{z - h}{z_T - h}, \quad z(\zeta) = h(x) + \zeta \frac{(z_T - h)}{z_T}; \quad h(x) \leq z \leq z_T$$

Physical Grid (x, z)



Computational Grid (x, ζ)



Terrain-Following z -Coordinates [2D Euler System]

- In the transformed (x, ζ) coordinates, the Euler 2D system becomes:

$$\frac{\partial}{\partial t} \begin{bmatrix} \sqrt{G}\rho' \\ \sqrt{G}\rho u \\ \sqrt{G}\rho w \\ \sqrt{G}(\rho\theta)' \end{bmatrix} + \frac{\partial}{\partial x} \begin{bmatrix} \sqrt{G}\rho u \\ \sqrt{G}(\rho u^2 + p') \\ \sqrt{G}\rho uw \\ \sqrt{G}\rho u\theta \end{bmatrix} + \frac{\partial}{\partial \zeta} \begin{bmatrix} \sqrt{G}\rho \tilde{w} \\ \sqrt{G}(\rho u \tilde{w} + G^{13}p') \\ \sqrt{G}\rho w \tilde{w} + p' \\ \sqrt{G}\rho \tilde{w} \theta \end{bmatrix} = \begin{bmatrix} 0 \\ 0 \\ -\sqrt{G}\rho'g \\ 0 \end{bmatrix}.$$

- Where the metric terms (Jacobians) and new vertical velocity \tilde{w} are

$$\sqrt{G} = \frac{dz}{d\zeta}, G^{13} = \frac{d\zeta}{dx}; \quad \tilde{w} = \frac{d\zeta}{dt} = \frac{1}{\sqrt{G}}(w + \sqrt{G}G^{13}u)$$

- The metric terms are time-independent (one time computation)
- Alternative formulations are also possible [e.g., Schär (2002), Klemp (2011)] for ζ , but the system of equations remains in flux-form.

$$\frac{\partial \mathbf{U}}{\partial t} + \nabla \cdot \mathbf{F}(\mathbf{U}) = \mathbf{S}(\mathbf{U}), \quad \mathbf{U} = [\sqrt{G}\rho', \sqrt{G}\rho u, \sqrt{G}\rho w, \sqrt{G}(\rho\theta)']^T$$

DG-NH, Explicit Time Stepping R-K Method

- Final form for the discretization leads to an ODE for each $U_{ij}(t)$:

$$\frac{\partial U}{\partial t} + \nabla \cdot \mathbf{F}(U) = S(U) \quad \Rightarrow \quad \frac{d}{dt} U_{ij}(t) = \frac{4}{\Delta x_i^1 \Delta x_j^2 w_i w_j} [I_{Grad} + I_{Flux} + I_{Source}]$$

- For a system of conservation laws, solve the decoupled ODE system:

$$\frac{d}{dt} U_h(t) = \mathcal{L}(U_h) \quad \Rightarrow \quad \frac{d}{dt} \mathbf{U}_h = L(\mathbf{U}_h) \quad \text{in } (0, T)$$

- Strong Stability Preserving third-order Runge-Kutta (SSP-RK) scheme (Gottlieb et al., SIAM Review, 2001)**

$$\begin{aligned} U^{(1)} &= U^n + \Delta t \mathcal{L}(U^n) \\ U^{(2)} &= \frac{3}{4} U^n + \frac{1}{4} U^{(1)} + \frac{1}{4} \Delta t \mathcal{L}(U^{(1)}) \\ U^{n+1} &= \frac{1}{3} U^n + \frac{2}{3} U^{(2)} + \frac{2}{3} \Delta t \mathcal{L}(U^{(2)}). \end{aligned}$$

where the superscripts n and $n+1$ denote time levels t and $t + \Delta t$, respectively

Time-Splitting Scheme: 'HEVI' Approach

- IMEX: Implicit solver for linear part and explicit solver for nonlinear parts. ¹
- HEVI:** Horizontal-Explicit-Vertical-Implicit. (**our focus**)

- Split into horizontal (x) and vertical (ζ or z) components:

$$(\text{Euler sys}) \quad \frac{\partial \mathbf{U}}{\partial t} + \frac{\mathbf{F}_x(\mathbf{U})}{\partial x} + \frac{\mathbf{F}_z(\mathbf{U})}{\partial z} = \mathbf{S}(\mathbf{U})$$

$$(\text{H-part}) \quad \frac{\partial \mathbf{U}}{\partial t} + \frac{\mathbf{F}_x(\mathbf{U})}{\partial x} = \mathbf{S}^x(\mathbf{U}) = (0, 0, 0, 0)^T$$

$$(\text{V-part}) \quad \frac{\partial \mathbf{U}}{\partial t} + \frac{\mathbf{F}_z(\mathbf{U})}{\partial z} = \mathbf{S}^z(\mathbf{U}) = (0, 0, -\rho' g, 0)^T$$

- The horizontal part may be solved explicitly.
- The vertical part may be solved implicitly.
- Connected by **Strang-type** time splitting, permitting $\mathcal{O}(\Delta t^2)$ accuracy.
 - One possible option is to perform " $H - V - H$ " sequence of operations.
 - Other possible option is " $V - H - V$ " sequence. Ideally, more expensive part should be solved only once.

¹Giraldo et al. (SIAM 2013)

Remarks on HEVI

To overcome $\bar{h} = \min\{\Delta x, \Delta z\} = \Delta z$

- Horizontal part explicitly using SSP-RK3.
 - Vertical part implicitly using Crank-Nicholson: one stage, second-order accurate.
-
- **Benefit:** The effective Courant number is only limited by the minimum horizontal grid-spacing $\min\{\Delta x, \Delta y\}$.
 - **Bonus:** The 'HEVI' split approach might retain the parallel efficiency of HOMME for NH equations too.
 - **Horizontal domain decomposition:** data accessible in the vertical direction.
 - Particularly useful for 3D NH modeling ($\Delta z : \Delta x = 1 : 1000$).
 - Global NH models adopt the HEVI philosophy².
 - Recent high-order FV-NH models based on operator-split method³.

²Satoh et al. (MWR 2008), Skamarock et al. (MWR 2012)

³Norman et al. (JCP, 2011), Ullrich et al. (MWR, 2012)

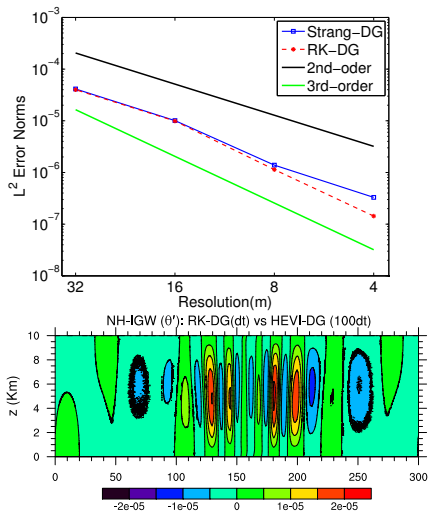
Inertia-Gravity Wave Test: 2D Channel Flow

- The evolution of a potential temperature perturbation θ' (K) in a channel having periodic lateral and no-flux top/bottom boundary conditions. [Skamarock & Klemp (1994)]
- Widely used for testing time-stepping methods in NH models, and $\Delta z \ll \Delta x$

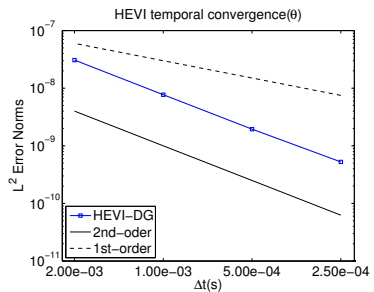
- Domain $[0, 300] \times [0, 10]$ km², T=3000 s. For $\Delta x/\Delta z = 10, 100$; $\Delta t = 0.14, 1.4$ s, respectively. For the reference solution (explicit), $\Delta t = 0.014$ s.
- Ref: *Bao, Kloefkorn & Nair (MWR, 2015)*

2D Inertia Gravity Wave: Convergence Study

HEVI-DG: Convergence with large aspect ratio (1 : 100)

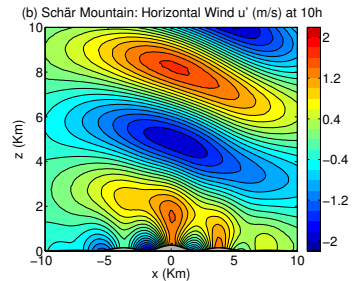
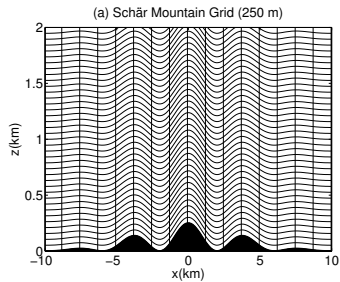
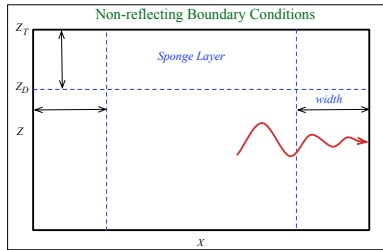


- $\Delta x = 100\Delta z$, i.e., 100 times larger Δt for HEVI-DG
- Difference field θ' is $O(10^{-5})$.
- 2nd-order temporal convergence with a smooth test case.



Mountain Wave Test: Schär Mountain ⁴

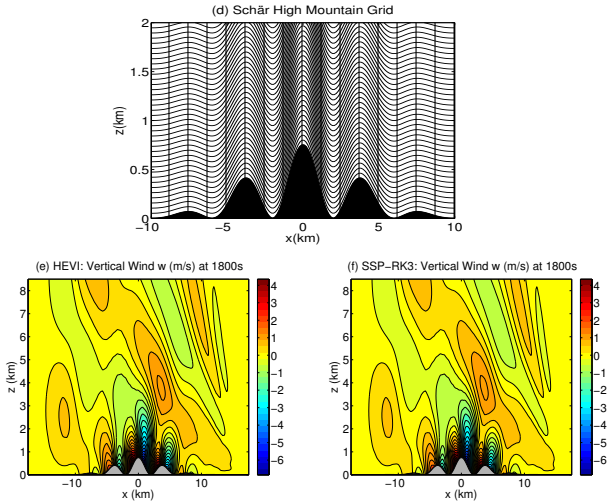
- P³-DG, vertical implicit solve by standard DG.
- Integrate for 10 h with $\Delta t = 0.125$ s.
- Domain $[-25, 25] \times [0, 21]$ km², $\Delta z = 105$ m, $\Delta x = 250$ m.
- Terrain-following height-based coordinate system
- Sponge layers on the lateral and top boundaries. No-flux BC at the bottom.



⁴Schär et al. (2002)

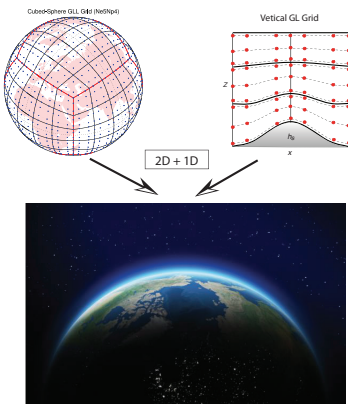
Schär High Mountain: HEVI vs Explicit

- Mountain with extreme elevation $h_0 = 750$ m (slope 55%)
- To test the robustness of HEVI as opposed to explicit RK [Bao, Kloefkorn & Nair 2014]



HOMAM: High-Order Multiscale Atmospheric Model

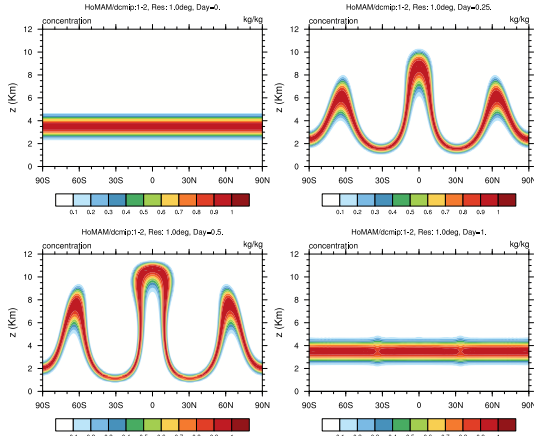
- Goal: To solve the 3D Euler System in curvilinear coordinates
- The computational domain \mathcal{D} is decomposed into 2D + 1D.
- Independent DG discretization in horizontal and vertical directions.
- HEVI time-stepping



- **Horizontal:** cubed-sphere surface, N_e^2 elements (N_p GLL points)
- **Vertical:** vertical grid line z or ζ , V_{nel} element (N_g GL points)
- **Total DOF:** $6N_e^2N_p^2 \times V_{nel}N_g$.

$$\begin{aligned} \frac{\partial \rho}{\partial t} + \frac{1}{\sqrt{G}} \left[\frac{\partial}{\partial x^j} (\sqrt{G} \rho u^j) \right] &= 0 \quad \{ \text{Summation Implied} \} \\ \frac{\partial \rho u^i}{\partial t} + \frac{1}{\sqrt{G}} \left[\frac{\partial}{\partial x^j} [\sqrt{G}(\rho u^i u^j + p G^{ij})] \right] &= -\Gamma_{jk}^i (\rho u^j u^k + p G^{jk}) \\ &\quad + f \sqrt{G}(u^1 G^{2i} - u^2 G^{1i}) - \rho g G^{3i} \\ \frac{\partial \rho \theta}{\partial t} + \frac{1}{\sqrt{G}} \left[\frac{\partial}{\partial x^j} (\sqrt{G} \rho \theta u^j) \right] &= 0 \\ \frac{\partial \rho q}{\partial t} + \frac{1}{\sqrt{G}} \left[\frac{\partial}{\partial x^j} (\sqrt{G} \rho q u^j) \right] &= 0. \end{aligned}$$

3D Advection Test: “Hadley-like” Meridional Circulation



- HEVI, HEVE and Full (un-split) produce visually identical results.

3D Advection Test (DCMIP-12): Convergence Study

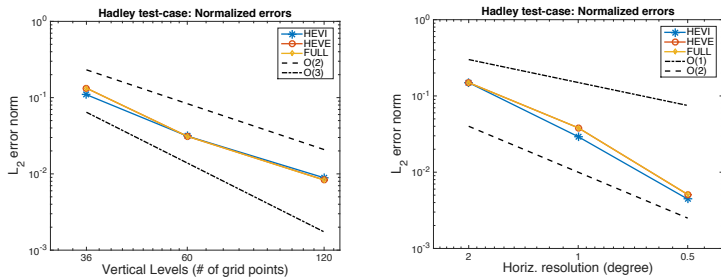


Table: Convergence Rate: DCMIP, Kent et al. (2014), Hall et al (2015) Average convergence rate for the normalized error norms for the Hadley test (DCMIP test 1-2) computed using resolutions $2^\circ, 1^\circ, 0.5^\circ$ horizontal, and respectively with 30, 60, 120 vertical levels.

Errors/Models:	Mcore	CAM-FV	ENDGame	CAM-SE	HOMAM
ℓ_1	2.22	1.93	2.18	2.27	2.62
ℓ_2	1.94	1.84	1.83	2.12	2.43
ℓ_∞	1.64	1.66	1.14	1.68	2.16

3D Nonhydrostatic Gravity Waves: DCMIP 3-1 Test

- NH Gravity Wave test (DCMIP-31) on a reduced planet ($X = 125$), θ' after 3600s
- $N_e = 25, N_p = 4, N_g = 4$ ($\Delta x \approx \Delta z \approx 1$ km), $\Delta t = 0.25$ s
- The initial state is hydrostatically balanced and in gradient-wind balance.
- An overlaid potential temperature perturbation triggers the evolution of gravity waves.

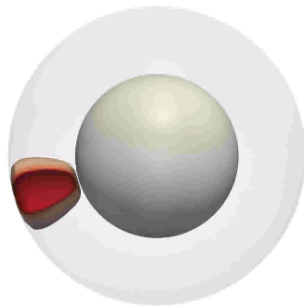
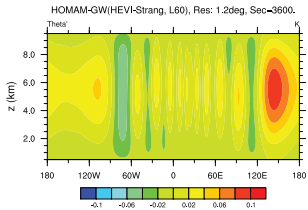
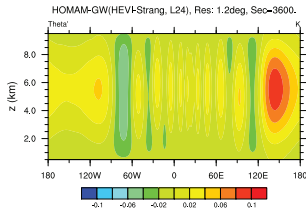
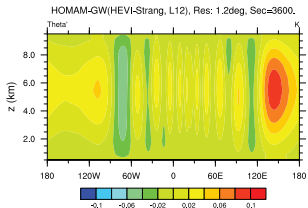
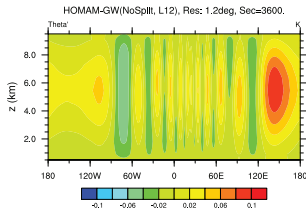


Figure: Screenshot of 3D IGW wave (*Blaise et al., 2015*)

DCMIP 3-1 Test: Varying the number of vertical levels

- Fix the horizontal resolution to 1 km. Vary the number of vertical levels such that $\Delta x / \Delta z = 1, 2, 5$.
- For HEVI-Strang, we use the same $\Delta t = 0.25$ s, not affected by the vertical resolution.



3D Nonhydrostatic Gravity Waves: HEVI vs Explicit

Table: Timing results of HEVI-Strang and SSP-RK3

RK scheme	$\Delta x/\Delta z$	Vertical Levels	Δt	Computing Time
SSP-RK3	1	12	0.25 s	91.0 s
HEVI-Strang		12	0.25 s	167.0 s (1.85)
SSP-RK3	2	24	0.125 s	356.0 s
HEVI-Strang		24	0.25 s	349.0 s (0.98)
SSP-RK3	5	60	0.05 s	2297.0 s
HEVI-Strang		60	0.25 s	1234.0 s (0.53)

- HEVI maintains the parallel scalability of HOMAM

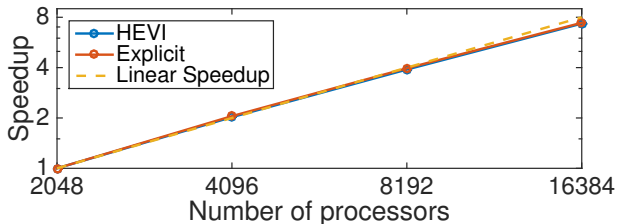


Figure: Strong Scaling

Summary

- Godunov-type FV method based on “AUSM⁺-up” numerical flux, combined with fifth-order 1D reconstructions (WENO5 and PQM) provides efficient local algorithms for global atmospheric modeling.
- Non-oscillatory advection, conservation and relaxed CFL make high-order Godunov-type FV a potential/promising candidate for NH modeling.

Discontinuous Galerkin Method (DGM)

- DGM with moderate order (third or fourth) is an excellent choice for atmospheric modeling, which addresses:
 - ① Local and global conservation with geometric flexibility on spherical grids. High-order accuracy and computational efficiency
 - ② Maintains the high parallel efficiency of HOMME framework
- The operator-split HEVI approach avoids stringent CFL restriction associated with vertical discretization, for NH model based on DG methods.
- Early results with the 3D global NH model (HOMAM, split and un-split) are promising, and it performs well under benchmark test cases.

Current & Future Research:

- Extending HOMAM in CAM-SE framework and validating with DCMIP-2016 benchmark tests
- More efficient time integration schemes are desirable for practical climate simulations.
Possible approaches: Multi-rate time integration in HEVI framework